IGBT Model Validation for Soft-Switching Applications

David W. Berning and Allen R. Hefner, Jr., *Senior Member, IEEE*

***Abstract*—Techniques are described for validating the performance of insulated gate bipolar transistor (IGBT) circuit simulator models for soft-switching circuit conditions. The circuits used for the validation include a soft-switched boost converter similar to that used in power-factor correction, and a new half-bridge testbed that is specially designed to examine the details of IGBT soft-switching waveforms. The new testbed is designed to emulate the soft-switching circuit conditions of actual applications circuits, while allowing the easy change of IGBT operating conditions. The testbed also eliminates the problems of commutating diode noise and IGBT temperature rise found in actual application circuits. Simulations of IGBT models provided in circuit simulator component libraries are compared with measurements obtained using these test circuits for the soft-switching conditions of zero-voltage turn-on, zero-voltage turn-off, or zero-current turn-off. Finally, the results are summarized by comparing the switching energies for the various measurements and simulations presented in this work.**

***Index Terms*—Circuit simulation, insulated gate bipolar transistor, model validation, power electronics, soft switching, switching energy.**

I. Introduction

THE insulated gate bipolar transistor (IGBT) is becoming the power switch of choice for many power applications because it offers a good compromise between on-state loss, switching speed and switching losses, and ease of use. The IGBT has enjoyed particularly deep penetration in the field of motion control where supply bus voltages range from 300 V to several times higher. To accommodate these voltages, a large variety of IGBTs are available today with a 600–1200 V blocking capability. Devices with higher voltage ratings are also being made by various manufacturers [1]. IGBTs are now offered both as single devices or packaged in modules with multiple IGBTs and/or diodes. Some modules include driver circuitry as well.

In recent years, efforts to model the switching behavior of IGBTs have been greatly expanded [2]–[8], [16]. In many cases, circuit modeling has become an economic necessity. The cost of the components and load of a medium to high-power circuit is so high that all means available must be used to lower the risk of system failure both during the prototyping phase of product development and production. Furthermore, substantial product quality and cost benefits can be obtained using IGBT circuit simulation. An assessment of the economic impacts of IGBT modeling is detailed in a recent study [9].

As the physics that govern transistor behavior are quite complex, attempts at accurately predicting the details of transistor switching performance tax compact models to their greatest extreme. Test procedures are needed that can be used to verify the predictions made by various models in order to check their validity, and these procedures need to be applicable to commonly used circuits. The NIST/IEEE Working Group on Model Validation [10] has been established to address the need for testing the validity of various models as they relate to predicting the behavior of devices under realistic conditions. The work presented in this paper is performed, in part, to support the needs of the IGBT task of the Working Group.

IGBTs are increasingly being used in soft-switching circuit applications in order to reduce switching loss [11]. Soft-switching operation is particularly appropriate for IGBTs in that much of the advantage that IGBTs have in low on-state voltage can be lost if these devices are used in hard-switching circuits. Various studies of IGBT internal device dynamics through simulation and measurement for soft-switching circuits have been undertaken previously [12], [13]. In previous model-validation studies, prototype public-domain versions of IGBT models have been used, and parameter extraction was performed by the authors. In this paper, the models and parameters provided in the Saber[1] [8] component libraries are used. System designers prefer the component library models because they provide a turnkey approach for modeling electronic systems. The component library models also represent the latest version of the model and parameter extraction procedures preferred by the software vendor.

Comprehensive test procedures are needed to validate IGBT models for soft-switching circuit applications. To validate a model, the model is tested for a variety of circuit conditions that are similar to those that may be encountered by different applications of the device being modeled. These tests should also be designed to be as insensitive as possible to errors that may be introduced by other circuit models. It is particularly important that these test procedures be built around a testbed

Paper IPCSD 00–061, presented at the 1999 Industry Applications Society Annual Meeting, Phoenix, AZ, October 3–7, and approved for publication in the IEEE TRANSACTIONS ON INDUSTRY APPLICATIONS by the Power Electronics Devices and Components Committee of the IEEE Industry Applications Society. Manuscript submitted for review October 15, 1999 and released for publication November 4, 2000. This work was supported in part by the Office of Microelectronics Programs.

The authors are with the Semiconductor Electronics Division, National Institute of Standards and Technology, Gaithersburg, MD 20899 USA (e-mail: david.berning@nist.gov; allen.hefner@nist.gov).

Publisher Item Identifier S 0093-9994(01)02110-7.

[1]Saber is a trademark of Avant!, Inc., previously Analogy, Beaverton, OR. Certain commercial products have been identified in order to specify or describe the subject matter of this paper adequately. In no case does this identification imply recommendation or endorsement by the National Institute of Standards and Technology, nor does it imply that the products are necessarily the best for the purpose.

U.S. Government work not protected by U.S. copyright.

that is well understood and well characterized so that the device model is given the correct information for the simulations. Furthermore, it is desirable to have specially designed circuits that: 1) isolate the important device characteristics and 2) allow the circuit parameters to be varied easily so that the device can be tested for a wide range of circuit conditions.

In this paper, the overall IGBT model performance for soft-switching conditions is examined using a boost converter circuit. The boost converter is commonly used for power-factor correction at medium- to high-power levels. Power-factor correction is rapidly becoming an important application for IGBTs, and soft-switching techniques work well in these applications. In Section II, a boost converter application circuit is described and IGBT current and voltage waveform measurements are made. Measurements using the boost converter are compared with simulations of this circuit using the models of specific IGBTs contained in the simulator component library.

To further examine IGBT model soft-switching performance in the critical transient regions of the voltage and current waveforms, a new testbed is presented in Section II. This circuit permits a wider variety of measurements to be made than possible with a single application circuit. This new testbed also largely avoids dependence of circuit behavior on other difficult-to-model devices such as diodes, and on temperature rise and noise. Measurements made on this testbed form the basis for the model-validation comparisons described in Section III.

II. Model Validation Circuits

Three different types of soft-switching conditions are commonly encountered by IGBTs in soft-switching power circuits: 1) zero-voltage turn-off, where the IGBT is turned off and a capacitor provides an alternate current path so that the IGBT anode voltage rise is slowed; 2) zero-voltage turn-on, where the IGBT gate is already on when positive anode voltage or current is applied; or 3) zero-current turn-off, where anode current is removed before the IGBT gate is turned off, and anode voltage is reapplied after the IGBT gate is turned off. The boost converter of Section II-A demonstrates the overall performance of an IGBT model for zero-voltage turn-off and zero-voltage turn-on. The specially designed testbed described in Section II-B is used in Section III to examine all three of the soft-switching conditions under a wide variety of circuit parameters and IGBT types.

A. Boost Converter

Fig. 1 is a schematic of a soft-switched boost converter similar to that used by the power section of a power-factor correction circuit. *Q1* is the main power device, and the waveforms are measured with respect to this device. *Q2* is the auxiliary switch, which implements the soft-switching aspect of this circuit. This circuit works in the following manner. Initially, both IGBTs are off and current is flowing through the 1.46-mH inductor *L1*, the commutation diode *D4*, and into the 10-μF output capacitor *C1*. For the model validation tests, output current is recirculated back to the power supply through the 2-Ω resistor *R3*, whereas the current would power a load in a real application. The auxiliary switch *Q2* is then turned on for a short period of time. This

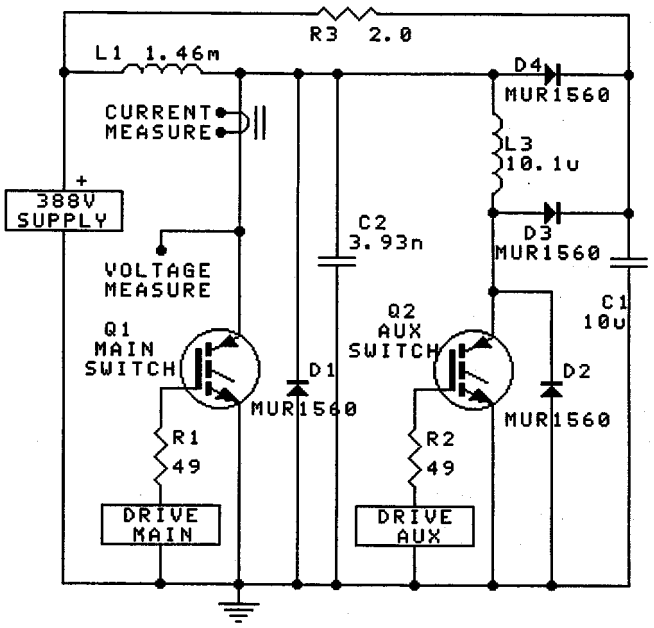

Fig. 1. Circuit used to both measure and simulate waveforms for the boost converter.

diverts the current from *D4* to the 10.1-μH inductor *L3*, and *D4* becomes reverse biased. *L3* forms a resonant network with the 3.93-nF snubber capacitor *C2*, causing the anode voltage on the main IGBT switch *Q1* to fall to a negative value, at which point *D1* begins to conduct. *Q1* is then turned on under zero-voltage and zero-current conditions. After the *Q1* turn-on, *Q2* is turned off, and the energy stored in the *L3* is recovered through *D3*. As *Q1* begins to conduct, the 1.46-mH inductor *L1* is recharged. At the end of the conduction period, *Q1* turns off and current is diverted to *C2*. This is the zero-voltage turn-off soft-switching event.

Fig. 2 shows the measured and simulated waveforms for the boost converter circuit given in Fig. 1. The model used for the simulations is one developed by Hefner [4], and run with a particular device in the Saber 4.0 component library [8]. The top graph shows the measured (solid) and simulated (dashed) anode voltage waveforms for *Q1*. The next two graphs show the gate drive signals for *Q1* and *Q2*, respectively. The bottom graph shows the measured and simulated anode current waveforms for *Q1*. There is good global agreement between the measurement and simulation. *Q1* and *Q2* are both medium-speed IGBTs, and the tail-current feature is visible in both current waveforms. This boost converter does allow one to test the IGBT model for these operating conditions, but it is difficult to change the circuit to test the model for a wide range of conditions. Furthermore, the circuit operates continuously and the IGBTs operate at an elevated temperature due to self-heating.

B. Soft-Switching Model-Validation Testbed

Fig. 3 is a block diagram of the new soft-switching IGBT model-validation testbed designed to test IGBT models for a wide range of well-controlled soft-switching conditions. Detailed circuit schematics for the testbed can be obtained by

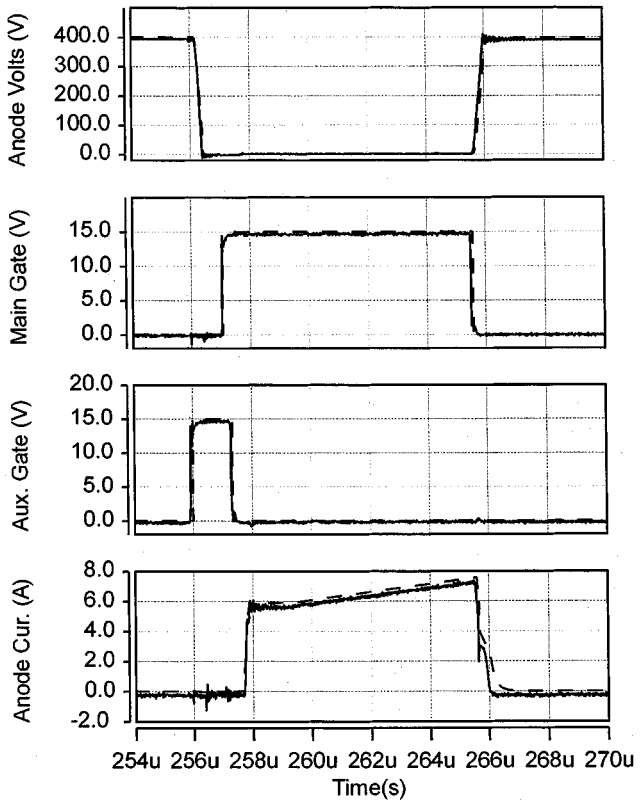

Fig. 2. Waveforms obtained from the boost converter of Fig. 1. The solid curves are the measured, and the dashed curves are the simulated, waveforms. The graphs show the following: 1) anode voltage; 2) main switch gate voltage; 3) auxiliary switch gate voltage; and 4) anode current.

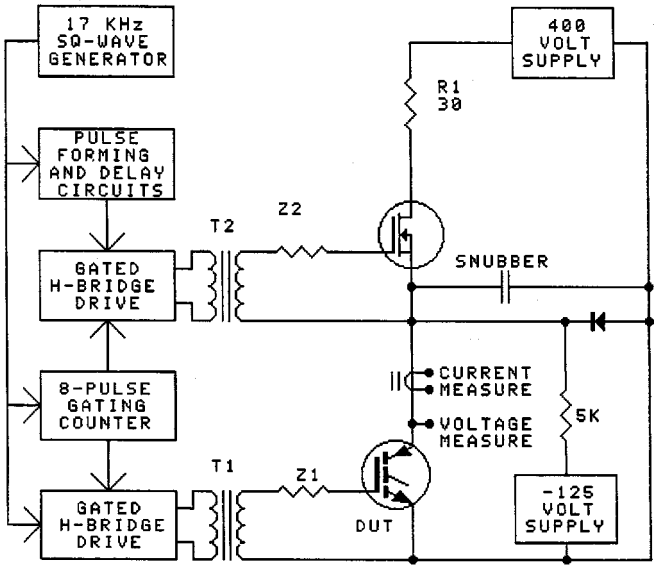

Fig. 3. Block diagram of soft-switch testbed with IGBT and associated components.

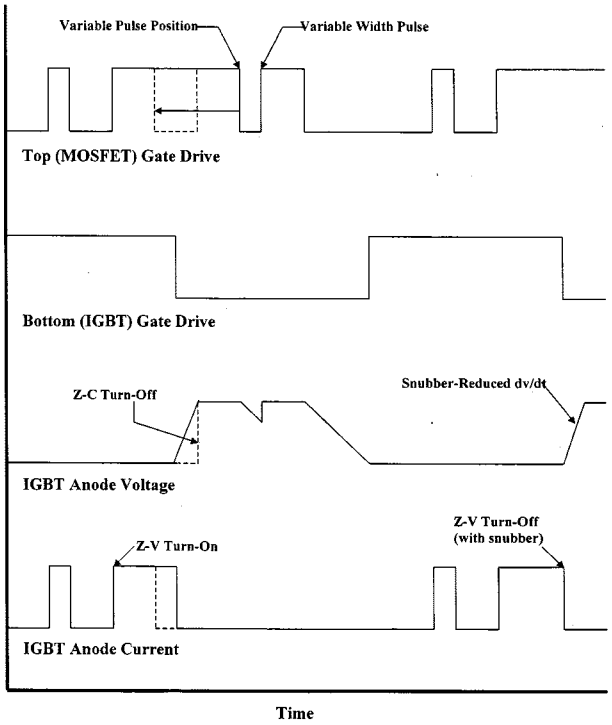

Fig. 4. Idealized waveforms for the soft-switching testbed.

contacting the authors directly. This testbed is an extension of the shoot-through/diode emulation testbed developed previously for validating IGBT models for hard-switched half-bridge circuit conditions [14], [18]. The new soft-switching circuit uses a MOSFET as the top device in a half-bridge to cause the IGBT to experience conditions similar to those that might be found in a variety of soft-switching applications. The MOSFET is turned on and off with a special double-pulsed waveform that has one of its pulses adjustable in width and position relative to the IGBT gate drive pulses. As the MOSFET gate pulse is delayed relative to the IGBT gate pulse, various IGBT soft-switching conditions are realized. An overall 50% duty cycle is maintained for both MOSFET and IGBT gate drives, as these signals are coupled through transformers. To avoid significant self-heating of the IGBT, the power portion of the circuit is activated for only 8 cycles at a very low burst rate.

Fig. 4 shows idealized waveforms for the new testbed. The top two waveforms show the gate drives for the MOSFET and IGBT, respectively. The drive for the MOSFET provides a movable pulse as shown, with the solid line indicating a pulse position set for making a zero-voltage soft-switching measurement. The dashed pulse indicates a pulse position set for making a zero-current turn-off measurement. The bottom two waveforms show the IGBT anode current and voltage, respectively. The three primary conditions of interest for soft switching are also indicated.

Fig. 5 shows the equivalent circuit of the testbed, which includes all of the parasitic elements, needed for accurate simulation. Parasitic elements include the 20-pF capacitor *C1*, the 9-nH cathode inductor *L4*, the 9-nH source inductor *L6*, and the 38-nH power supply inductance *L3*. Gate inductance for both the MOSFET and the IGBT are lumped into the leakage inductance of the gate-drive transformers. Each of these inductances is 99 nH.

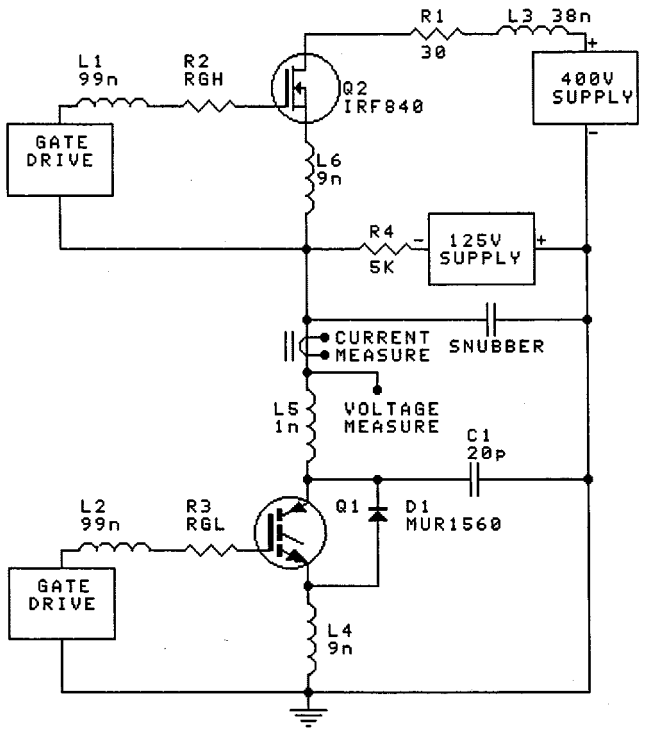

Fig. 5. Model validation testbed, including parasitics.

The negative 125-V power supply and 5-kΩ resistor of Fig. 5 are used to establish a forward bias in the anti-parallel diode placed across the IGBT to more closely approximate the conditions present in soft-switching applications. The forward diode current is much less than it would be in a typical application, and thus any errors introduced by the diode model used in the simulation are minimized. The measured and simulated IGBT current includes the anti-parallel diode current. The testbed is constructed with the diode in close proximity to the IGBT for noise considerations, and the current probe can not easily be placed to allow the IGBT current to be measured separately. A 30-Ω current-limiting resistor *R1* is used for all measurements and simulations.

Gate series resistors *RGH* and *RG*L are circuit variables that are changed to obtain different conditions. For the soft-switched measurements described in this paper, *RGL* is 13 Ω. Most measurements use a value of 43 Ω for *RGH*, but this value is altered for different zero-voltage turn-on measurements. The snubber capacitor is used for the zero-voltage turn-off conditions, but it is not used for the other conditions. The 1-nH inductor *L5* is simply a reference part defined in the simulation circuit for the purpose of referencing the current. All voltage measurements are taken at the anode of the IGBT.

III. Model Validation Results

Physics-based IGBT models are presently provided within commercial circuit simulator software. Saber 4.0 [8] is one such simulator, and this software includes both the buffer-layer [4] and nonbuffer-layer [2] IGBT models developed by Hefner, as well as an electrothermal version of each model [5], [17]. One methodology for using these models is for the user to extract the required model parameters from a series of well-specified laboratory procedures [4], [15]. Because the process of extracting these parameters is not trivial, most users of commercial circuit simulators are not able to extract these model parameters themselves and depend on the software vendor providing an array of fully specified library components. Great effort is underway to have as many of the current IGBTs represented in these libraries as possible. In this paper, models provided in simulator component libraries are used for all validation results.

In this section, simulated waveforms using IGBT models provided in simulator component libraries are compared with experimental results for various soft-switching conditions. The IGBTs include a standard-speed device, fast device, and an ultrafast device. For both the measurements and simulations, the devices operate at the realistic current and voltage levels of 13 A and 400 V for these 600-V 25-A IGBTs at both 25 °C and 100 °C. Before the soft-switching validation results are described, it is informative to examine an example case of hard-switching model validation.

A. Hard Switching

Techniques for model validation for IGBTs operating in a half-bridge were previously published [14]. Model parameters were extracted using a series of measurements in this previously published work, rather than using library-described parts. An example is now given in this paper of model-validation waveforms obtained in the half-bridge testbed described in [14], but using the same ultrafast IGBT that is described in the library and used later for the soft-switching validation.

IGBT operation in soft-switched circuits presents a somewhat different set of issues than it does in hard-switched circuits. In hard-switched circuits, the IGBT gate is switched either on or off, and the anode voltage or current is switched with certain delay and speed characteristics that depend on device parameters and gate-drive impedance. In soft-switching applications, the timing of the turn-off or turn-on of anode current, as well as current and voltage waveforms, are partially circuits dependent rather than being mostly device dependent.

The following hard-switching example is shown to demonstrate the level of agreement between model and experiment in terms of the IGBT gate current and voltage waveforms, and switching delay. These parameters are not examined in the soft-switching validation procedure and are, thus, examined in the following example for completeness.

Fig. 6 shows the waveforms for turn-on of an ultrafast IGBT. The top waveform shows the gate drive voltage applied to a 130-Ω gate resistor, and the next two waveforms show actual gate voltage and current, respectively. The remaining waveforms show anode voltage and anode current. The measured waveforms are shown as solid lines, and the simulated ones are dashed. The very small discrepancy between the measurement and the simulation with regards to delay and gate current indicates that the model describes the input characteristics of the IGBT very well.

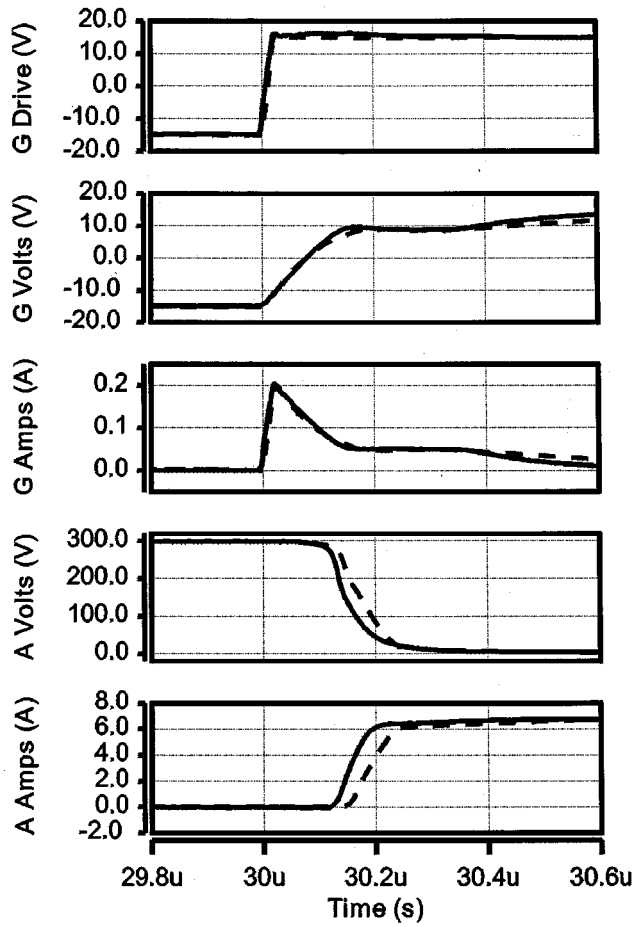

Fig. 6. Sample comparison between measured (solid) and simulated (dashed) waveforms for hard switched ultrafast IGBT turn-on.

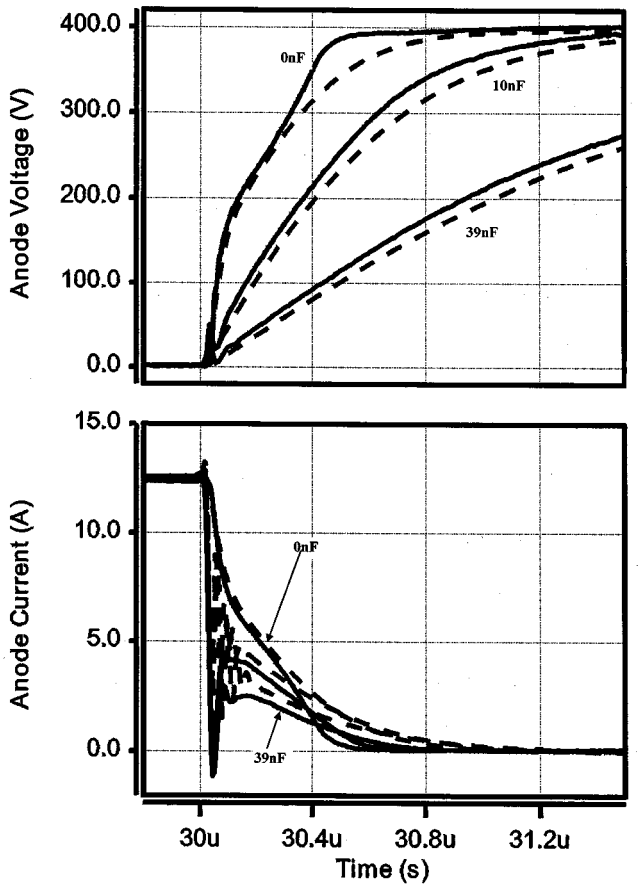

Fig. 7. Comparison between measured (solid) and simulated (dashed) waveforms for zero-voltage turn-off of the fast IGBT with different amounts of snubbing at 25°.

B. Zero-Voltage Turn-Off

The zero-voltage turn-off conditions described in this section are realized by switching the IGBT off from an initial state of load-current conduction. The MOSFET in the testbed circuit remains on for the entire time, and the initial IGBT current is determined by the 30-Ω load resistor and the 400-V power supply. Zero-voltage turn-off occurs when an added snubber capacitor diverts part of the IGBT current as the anode voltage is rising.

Fig. 7 shows anode current and voltage waveforms for the fast IGBT for various zero-voltage turn-off conditions for a temperature of 25 °C. The fastest voltage-rise waveform is recorded with no snubber capacitor, and actually represents a hard-switching event. The remaining voltage waveforms, in order, show zero-voltage turn-off with 0.01- and 0.039-μF snubber capacitors. The measured waveforms are solid curves and the simulated ones are dashed. A greater amount of snubbing reduces the amplitude of the tail current, but increases the length of the tail. Both measurements and simulations show a factor of about six for reduction in switching loss in this IGBT when changing from hard switching to zero-voltage turn-off using the 0.039-μF snubber capacitor. The switching-loss values are listed in Table I.

The simulated switching-energy values show reasonable agreement with the measured values. These simulations are a severe test of the model in general, and of the exactness of the parameter extraction in particular. Rather minor changes in model parameters can make large changes in these transient waveforms and the corresponding switching energies. It is easy to change a parameter in the model to cause excellent agreement between measurement and simulation for a given switching condition, but this will likely cause some other problem, such as an incorrect on-voltage.

Fig. 8 shows the anode current and voltage waveforms for the same device and switching conditions as shown in Fig. 7, but with the IGBT case temperature at 100 °C. The higher temperature causes both the amplitude and the length of the current tail to increase. Both the measurements and the simulations show these trends.

The anode voltage and current waveforms for various turn-off conditions for the ultrafast IGBT are shown in Fig. 9. These data are taken for a case temperature of 25 °C. The fastest anode-voltage-rise waveform is recorded with no snubber capacitor. The remaining voltage waveforms, in order, show zero-voltage turn-off with 0.0039- and 0.01-μF snubber capacitors. The measured waveforms are solid curves and the simulated ones are dashed. The shapes of these curves are similar to those for the fast IGBT, however, the time scale is

TABLE I
EXPERIMENTAL AND SIMULATED IGBT SWITCHING ENERGIES FOR VARIOUS SOFT-SWITCHING CONDITIONS

Device and Conditions	Exp.	Sim.
Group 1		
ZV turn-off, fast, no snub, 25 °C	407μJ	585μJ
ZV turn-off, fast, 0.01μF, 25 °C	185μJ	288μJ
ZV turn-off, fast, 0.039μF, 25 °C	64μJ	100μJ
ZV turn-off, fast, no snub, 100 °C	685μJ	1004μJ
ZV turn-off, fast, 0.01μF, 100 °C	405μJ	463μJ
ZV turn-off, fast, 0.039μF, 100 °C	166μJ	187μJ
Group 2		
ZV turn-off, ultra, no snub, 25 °C	129μJ	75μJ
ZV turn-off, ultra, 0.0039μF, 25 °C	52μJ	34μJ
ZV turn-off, ultra, 0.01μF, 25 °C	26μJ	18μJ
Group 3		
ZV turn-off, stand, no snub, 25 °C	2910μJ	2780μJ
ZV turn-off, stand, 0.047μF, 25 °C	1861μJ	1603μJ
ZV turn-off, stand, 0.1μF, 25 °C	1458μJ	1096μJ
ZV turn-off, stand, 0.33μF, 25 °C	862μJ	495μJ
Group 4		
ZC turn-off, fast, 1200ns win., 25 °C	22μJ	36μJ
ZC turn-off, fast, 1200ns win., 100 °C	149μJ	93μJ
ZC turn-off, fast, 400ns win., 25 °C	121μJ	220μJ
ZC turn-off, fast, 400ns win., 100 °C	358μJ	394μJ
Group 5		
ZC turn-off, ultra, 400ns win., 25 °C	11μJ	9μJ
ZC turn-off, ultra, 400ns win., 100 °C	51μJ	10μJ
Group 6		
ZC turn-off, stand, late off, 25 °C	462μJ	115μJ
ZC turn-off, stand, early off, 25 °C	1310μJ	775μJ
ZC turn-off, stand, late off, 100 °C	1510μJ	600μJ
ZC turn-off, stand, early off, 100 °C	2628μ J	1990μJ
Group 7		
ZV turn-on, ultra, 50A/μs, 25 °C	10.5μJ	7.3μJ
ZV turn-on, ultra, 150A/μs, 25 °C	15μJ	4.8μJ
ZV turn-on, ultra, 600A/μs, 25 °C	22μJ	5.1μJ
ZV turn-on, ultra, 175A/μs, 25 °C	18.7μJ	4.8μJ
ZV turn-on, ultra, 175A/μs, 100 °C	31.6μJ	7.0μJ

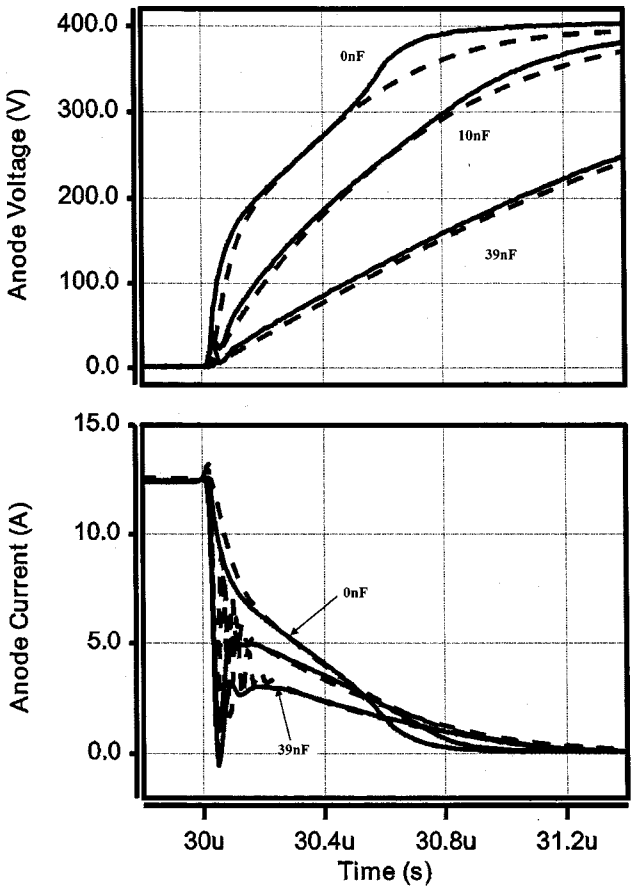

Fig. 8. Comparison between measured (solid) and simulated (dashed) waveforms for the same conditions as those shown in Fig. 7, but at 100°.

reduced. The corresponding switching-loss energies also show similar trends, but the ultrafast IGBT has lower losses.

Fig. 10 shows the anode current and voltage waveforms for the standard-speed IGBT at a temperature of 25 °C. The fastest anode-voltage-rise waveform is recorded with no snubber capacitor. The remaining voltage waveforms, in order, show zero-voltage turn-off with 0.047-, 0.1-, and 0.33-μF snubber capacitors. The measured waveforms are solid curves and the simulated ones are dashed. It is interesting to note that the largest difference between the simulation and the experiment occurs with the largest snubber capacitor for this IGBT. It might be expected that the simulation would be closest to the experiment for this relatively large capacitor since the anode-voltage waveform is almost totally dominated by the capacitor. However, the largest difference in the current waveforms occurs near the end of the tail, and the larger values of snubber capacitance prolong the tail region.

C. Zero-Current Turn-Off

The zero-current turn-off conditions described in this section are realized by a sequence of three events. Referring again to Figs. 4 and 5, initially both the MOSFET and IGBT are on, and the load resistor and power supply determine the IGBT current. First, switching off the MOSFET interrupts the IGBT anode current. Secondly, the IGBT gate is turned off. Finally, the MOSFET is turned back on to reapply voltage to the IGBT. A tail-current bump occurs when the anode voltage is reapplied if the carriers in the IGBT have not had time to fully recombine.

The measurements and simulations given in this section examine this tail-current bump. As in the previous section, three different device types are examined at two different temperatures. There are two other parameters that are varied to affect this tail-current bump. One parameter is zero-current window width, which is defined as the time duration between when the MOSFET interrupts the IGBT current and when the MOSFET reapplies voltage to the IGBT.

The other parameter is used to describe the IGBT gate turn-off timing relative to the zero-current window. This parameter most strongly affects the current-tail bump size for the standard-speed IGBT, and this parameter is labeled “early off” or “late off.” Early off means that the IGBT gate is turned off just after the anode current is interrupted by the MOSFET. Late off means that the IGBT gate is turned off just before the anode voltage is reapplied by turn-on of the MOSFET. This parameter is not specified for the data given for either the fast or ultrafast device. For these devices, the IGBT gate is turned off 200 ns after the IGBT anode current is interrupted by the MOSFET.

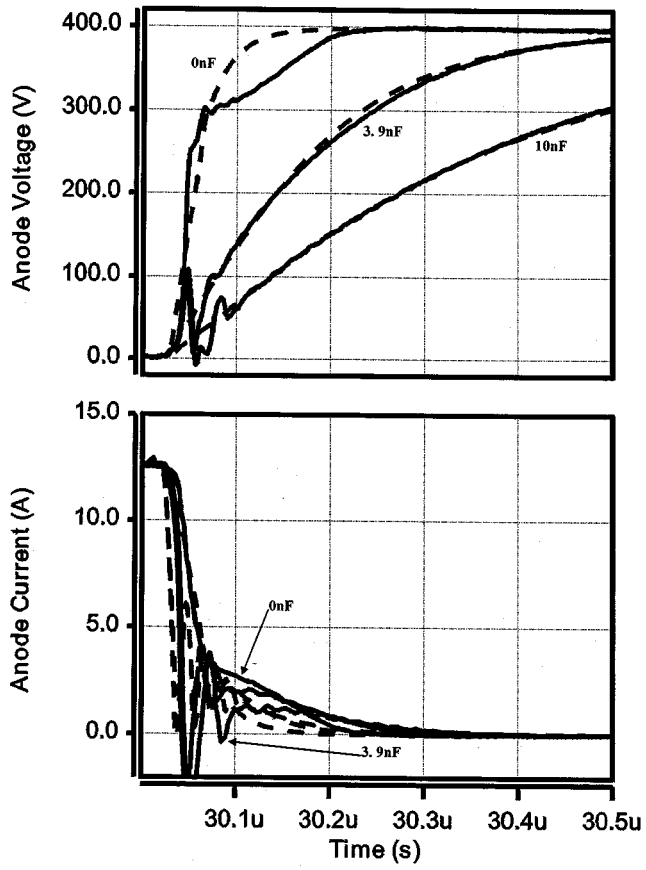

Fig. 9. Comparison between measured (solid) and simulated (dashed) waveforms for zero-voltage turn-off of the ultrafast IGBT with different amounts of snubbing.

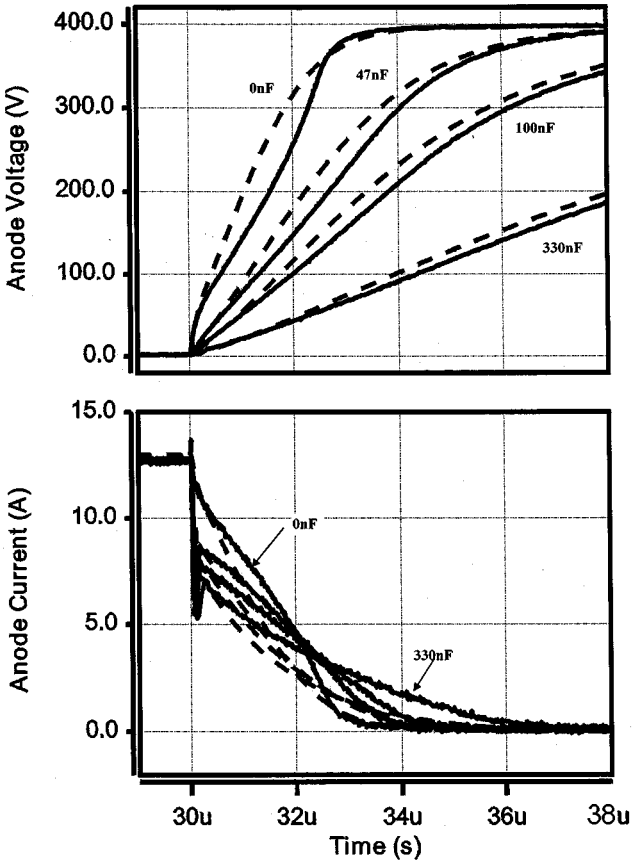

Fig. 10. Comparison between measured (solid) and simulated (dashed) waveforms for zero-voltage turn-off of the standard-speed IGBT with different amounts of snubbing.

Fig. 11 shows measured (solid) and simulated (dashed) waveforms for the fast IGBT under zero-current turn-off conditions. Data are shown for both 25 °C and 100 °C, and also for both 400- and 1200-ns window widths. The bottom graph in the figure shows the anode current, and the initial transition to zero current is the result of the MOSFET being turned off. The first current-bump cluster represents the 400-ns window-width condition, and the second bump cluster the 1200-ns window-width condition. The middle graph shows the anode voltage, and the top graph shows the IGBT gate drive voltage applied to the 13-Ω gate resistor for the 1200-ns window condition. The gate drive waveforms are not shown for the 400-ns window condition as they simply fall on top of the pair that is shown. The current-tail bumps are larger for the narrower window width, and also larger for the higher temperature. The measured and simulated results exhibit similar trends, and the corresponding switching energies are in reasonable agreement.

Zero-current turn-off measured (solid) and simulated (dashed) waveforms for the ultra-fast IGBT are shown in Fig. 12. Data are given for both 25 °C and 100 °C, and the window width is 400 ns. It is interesting to note that the size of the current-tail bump is affected strongly by temperature in the measurement, while the simulation shows little difference in bump size for the two different temperatures. The switching-energy table shows good agreement between the measured and simulated switching energies at 25 °C, but not at 100 °C. Furthermore, except for the measured 100 °C case, the energies are quite low, and it is likely that these bumps are due mainly to capacitive charging. The simulations usually have their largest errors toward the end of the current tails, and it appears that in the simulation, recombination is complete by the time the MOSFET turns back on, while in reality stored charge is still present in the 100°C case.

Fig. 13 shows zero-current turn-off data for the standard-speed IGBT. The window width is now 3 μs, and two different IGBT gate-turn-off positions are used. Again, the measured data are represented by the solid curves and the simulated data are shown as dashed curves. The temperature is 25 °C. The top graph shows the two different IGBT gate-turn-off positions that fall within the zero-current window. This window is visible in the anode-current graph at the bottom of the figure. Both measured and simulated results show a much larger current-tail bump when the IGBT gate is turned off early in the zero-current window, rather than late in the window. This is due to discharging base charge through reverse conduction in the MOSFET channel. Clearly, leaving the IGBT gate on as long as possible during the zero-current window is helping to reduce the recovery time for the device during turn-off. It is apparent from the energy table that the largest relative error

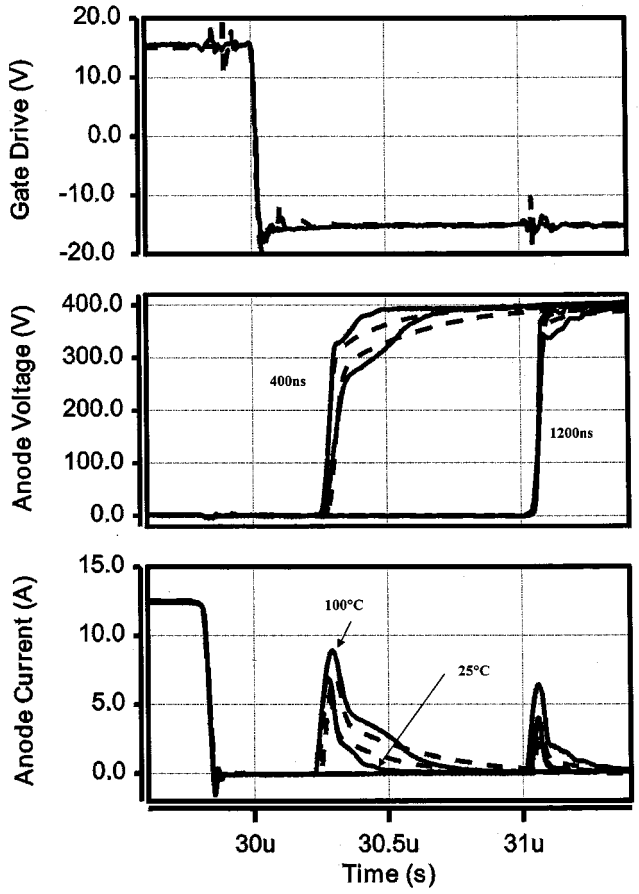

Fig. 11. Comparison between measured (solid) and simulated (dashed) waveforms for zero-current turn-off of the fast IGBT. Data are shown for 400-ns and 1200-ns window widths, and 25° and 100°.

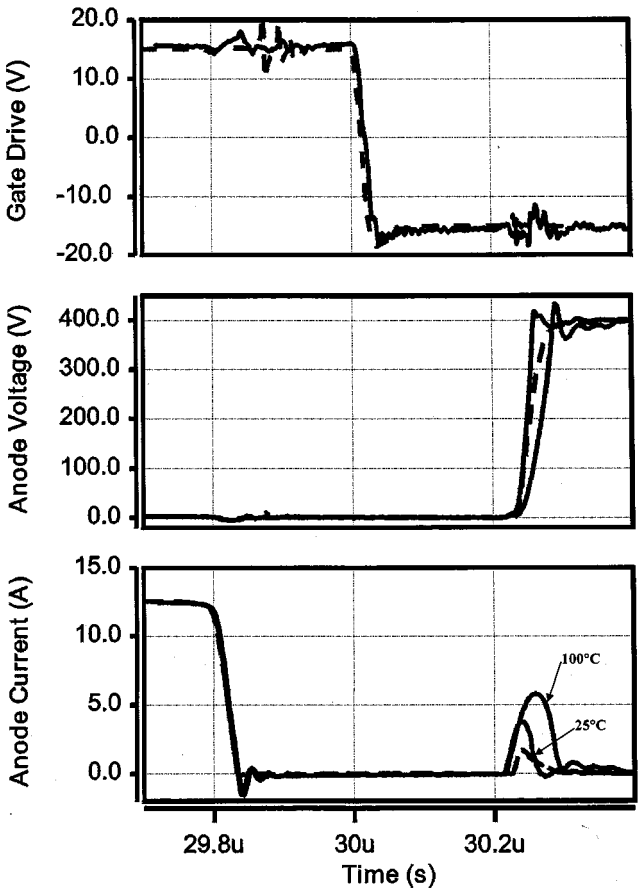

Fig. 12. Comparison between measured (solid) and simulated (dashed) waveforms for zero-current turn-off of the ultrafast IGBT at 25° and 100°.

in the simulation occurs when the energies are smaller. This is consistent with the observation of larger errors at the end of current tails mentioned above, in that in both cases the recovery of the IGBT is nearing completion.

The zero-current turn-off data for the same device and conditions shown in Fig. 13 are presented in Fig. 14, except that the temperature is 100 °C. The same trends are apparent in this figure and in the table, in that when the device is further away from complete recovery, the error in the simulation is smaller and the energies are larger.

D. Zero-Voltage Turn-On

The zero-voltage turn-on condition described in this section is realized when the IGBT gate is already on and anode current is suddenly applied to the device. Before the current is applied, the anode voltage is slightly negative per the forward-biased antiparallel diode and negative-biasing current source shown in Fig. 5. When the current is applied, by switching on the MOSFET, the IGBT voltage rises to its on-state voltage. Generally, there is an anode-voltage overshoot that occurs before the on-state voltage is reached. One important parameter that affects the amplitude of the overshoot is the rate of current application di/dt. This voltage overshoot is examined with both measurements and simulations in this section for the ultrafast device at both 25 °C and 100 °C, and for a range of di/dt values. Similar measurements and simulations for the standard-speed and fast devices produced similar results, but are not presented in this paper. It will be mentioned here that the slower devices have somewhat lower voltage overshoot values.

Fig. 15 shows measured (solid) and simulated (dashed) waveforms for three different di/dt values at a temperature of 25 °C. The anode currents are shown in the bottom graph, and the smallest di/dt is 50 A/μs, the middle di/dt is 150 A/μs, and the highest di/dt is 600 A/μs. The beginning point for the current rise has no significance for this analysis; it simply represents different delays for MOSFET turn-on due to the use of three different gate resistors (*RGH* in Fig. 5). The value of *RGH* affects di/dt, and the three corresponding values of gate resistors used are (in order) 200, 43, and 10 Ω.

The anode voltage is shown in the top graph. As the di/dt increases, the voltage overshoot becomes larger and narrower. The measured "switching" energies are also larger for the higher di/dt values. It can be seen from the graph that the simulation does show the same trends in overshoot amplitude and width, but falls well short of predicting the actual amplitudes. These large overshoots are difficult to understand, as they are much larger than would be predicted given a pure MOSFET device with no bipolar component having the same area and blocking

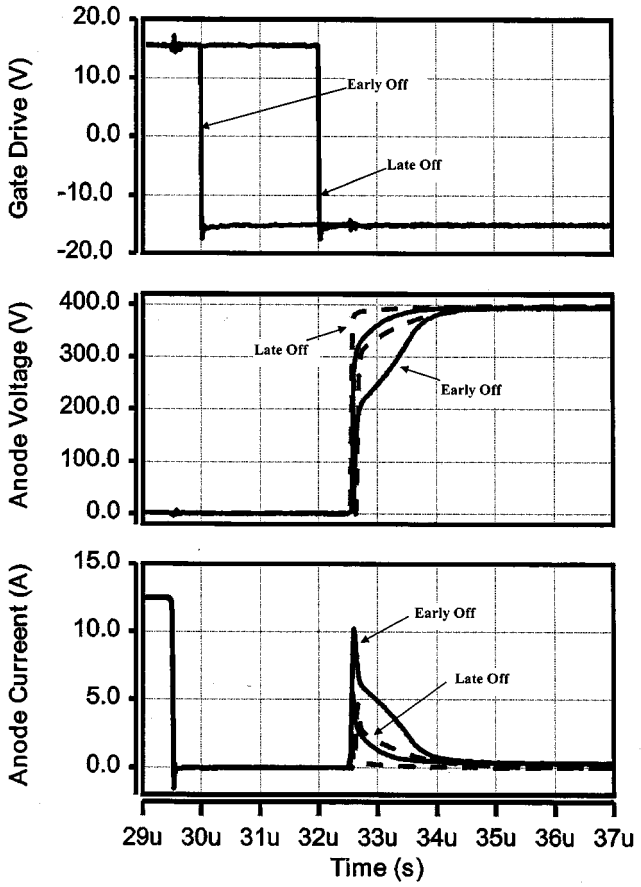

Fig. 13. Comparison between measured (solid) and simulated (dashed) waveforms for zero-current turn-off of the standard-speed IGBT at 25°. The IGBT gate is turned off at two different positions within the zero-current window.

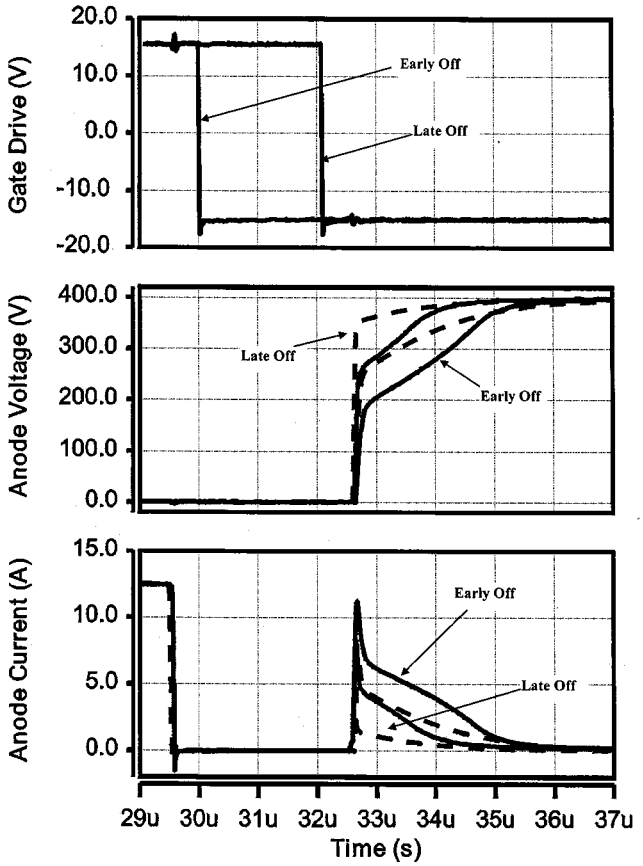

Fig. 14. Comparison between measured (solid) and simulated (dashed) waveforms for the same conditions as those shown in Fig. 13, but at 100°.

voltage. The overshoot is not observed when a MOSFET is substituted for the IGBT in the testbed.

Fig. 16 shows the temperature dependence of the di/dt-related voltage overshoot for a di/dt value of 175 A/μs. Both the measurements and the simulations show about a 50% increase in the voltage overshoot as the temperature is increased from 25 °C to 100 °C. This increase is consistent with an increase in on-resistance in the MOSFET part of the IGBT structure.

IV. Discussion and Analysis

A summary of the experimental and simulated switching energies is presented in Table I. The general organization of Table I is such that the results are presented in the order that they were described in the previous section. In this section, general trends will be extracted from the data presented in the table, including the effect of temperature, device speed, and type of switching. Trends in simulation error will also be discussed.

The first group of six entries in the table represents zero-voltage turn-off for the fast IGBT. Experimentally, increasing the temperature from 25 °C to 100 °C increases the switching energy by a factor of 2 to 3 when soft-switched, and less than a factor of 2 when hard-switched. The simulations indicate a fairly consistent factor of slightly less than 2 in energy for this same temperature change for both the hard- and soft-switched cases. The switching energies are reduced as the amount of snubbing is increased. The factors for this reduction when proceeding from the hard-switched case to the largest snubber case are given as follows. Experimentally, at 25 °C this factor is 6.4. In the simulation it is 5.6 at the same temperature. Experimentally, at 100 °C this factor is 4.1, and, in the simulation, it is 5.4.

The second group of three entries in the table presents similar data for the ultrafast IGBT at 25 °C. For both the measurements and the simulations, the switching energies are much smaller for the ultrafast IGBT than they are for the fast device. Experimentally, the factor in reduction is 3.2 for the hard-switched case and 3.6 for the case with the 0.01-μF snubber. The simulation indicates corresponding values of 7.8 and 8.5. Relatively minor changes in tail length or size make these differences seem quite large. Experimentally, for the ultrafast IGBT, the switching energy is reduced by a factor of 5 between the hard-switched case and the case with maximum snubbing. The simulation indicates a factor of 4.2 for this reduction over the same range of snubbing.

The third group of four entries presents data for the zero-voltage turn-off for the standard-speed IGBT. Experimentally, with no snubbing, this IGBT has a factor of 7.1 higher switching loss than the fast IGBT, while the simulation gives a factor of 4.8. Even when a large snubber capacitor is used with the standard IGBT, experimentally, there is more

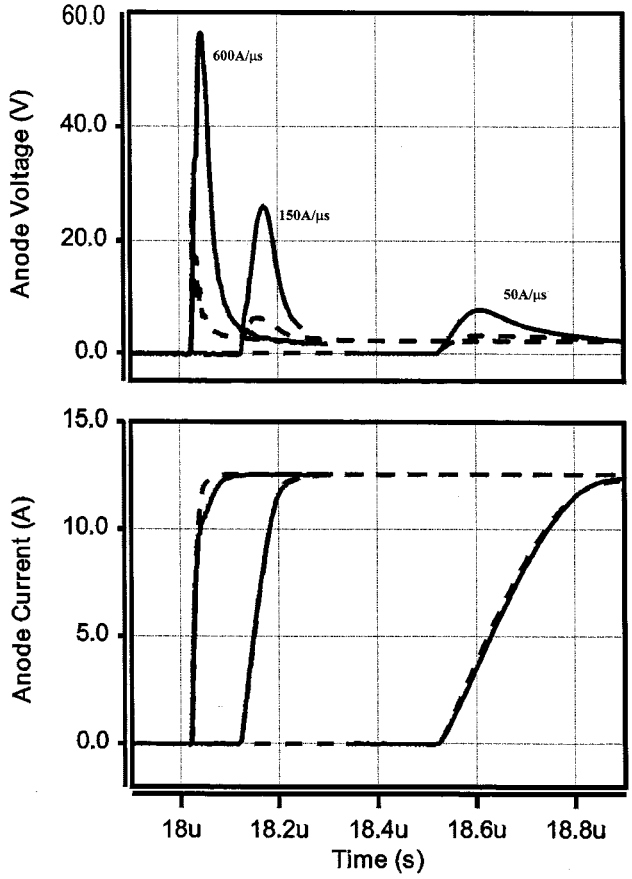

Fig. 15. Comparison between measured (solid) and simulated (dashed) waveforms for zero-voltage turn-on of the ultrafast IGBT at 25°. Three different values of di/dt are applied to the IGBT.

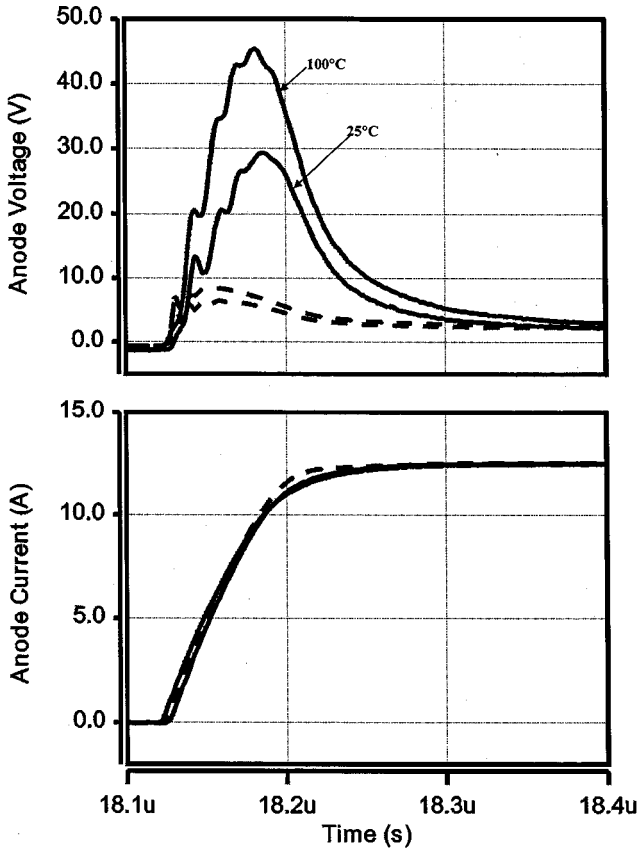

Fig. 16. Comparison between measured (solid) and simulated (dashed) waveforms for zero-voltage turn-on of the ultrafast IGBT at 25° and 100°.

switching-energy loss than there is for the fast IGBT in the hard-switched case. Experimentally, switching loss is reduced by a factor of 3.4 when the largest snubber capacitor is used compared to the hard-switched case. The simulation shows a factor of 5.6 in energy loss over this same range of snubbing.

The fourth group of table entries shows energy loss for the fast IGBT operating under zero-current turn-off conditions. Not surprisingly, switching energy is reduced when a longer zero-current window is used, both experimentally and in the simulations. In general it can be said that the turn-off loss is less with the zero-current turn-off than it is with the zero-voltage turn-off, assuming an adequately wide zero-current window is used.

When making comparisons in the switching-energy data for these soft-switching tests, it is important to be able to separate real trends from effects that can be misleading. For example, consider that experimentally there is a jump from 22 to 149 μJ of switching energy as the temperature is raised from 25 °C to 100 °C. This represents a factor of 6.8, but it would be incorrect to conclude that IGBT switching loss goes up by a factor of 6.8 with this temperature increase in general. In the analysis of the zero-current turn-off, whether by measurement or simulation, only a narrow slice of time is being considered, and this interval occurs some time well after the anode current is removed from the IGBT. In this case, there is still charge that has not recombined when the temperature is 100 °C at the point in time that the anode voltage is reapplied, whereas the charge has largely recombined under the same conditions at 25 °C. This type of effect also greatly magnifies differences between measured and simulated results because the details of the IGBT current tail are so difficult to accurately simulate. This effect demonstrates the difficulty that is to be expected when validating models under certain soft-switching conditions.

This difficulty is clearly shown in the fifth group, which shows the temperature effect on switching energy for the ultra-fast IGBT. Some tail current is present in the measurement at 100 °C, but this is not picked up in the simulation. The lowest turn-off losses are achieved by using zero-current turn-off with the ultrafast IGBT for the entire group of devices and conditions studied.

The sixth group of table entries is for the zero-current turn-off condition using the standard-speed IGBT. The highest relative error in the simulation occurs for the lowest energies, which is again indicative of the difficulty of predicting switching energy by observing only the final part of the recovery of the IGBT when most of the recovery takes place in the zero-current window region.

The seventh group of table entries lists switching energies for zero-voltage turn-on of the ultra-fast IGBT. The measured zero-voltage turn-on energies are on the same order as the various soft-switched turn-off energies for this device, whereas the simulation indicates that the turn-on energies are somewhat lower. For the slower devices (not shown), the turn-on energies are

much less than the turn-off energies, both experimentally and in the simulations.

Overall, the agreement between the measured and simulated energies shown in the table is reasonably good. In cases where large differences exist, they are usually attributable to situations where minor differences in the current-tail waveform result in a threshold effect, whereby the last portion of the IGBT recovery is disproportionately dominating the switching-energy values.

V. Conclusions

Techniques and examples have been given for validating IGBT models for various soft-switching circuits. The soft-switching boost converter was given as an application circuit that can be used for certain validation tests, and a validation example was shown using such a circuit. A more versatile testbed was also proposed that can be used for making a wider range of soft-switching model-validation tests on IGBTs. Several examples of the use of this circuit were given, and experimental and simulated waveforms were compared.

Both experimental and simulated switching energies for various soft-switching conditions were summarized in Table I. Appropriate soft-switching techniques can reduce both experimental and simulated switching energy losses in the IGBT by as much as an order of magnitude or more. Both measured and simulated results indicate that zero-current turn-off losses in the IGBT can be reduced by carefully choosing the gate timing so that the gate is turned off as late as possible in the zero-current window. Both measured and simulated results indicate that the zero-voltage turn-off condition implemented with a snubbing capacitor produces less switching loss in the IGBT than a hard turn-off, but slightly lower losses can be obtained with the zero-current turn-off circuit. Experimentally, zero-voltage turn-on of the IGBT results in a substantial voltage overshoot that is somewhat higher than predicted in the simulations, but the simulations do show the correct trends for temperature dependence, device speed, and rate of applied current.

References

[1] E. R. Motto and M. Yamamoto, "HVIGBT or GCT-Which is best," *PCIM Mag.*, pp. 36–44, May 1999.

[2] A. R. Hefner and D. M. Diebolt, "An experimentally verified IGBT model implemented in the saber circuit simulator," in *IEEE Trans. Power Electron.*, vol. 9, Sept. 1994, p. 532.

[3] R. Kraus and K. Hoffmann, "An analytical model of IGBT's with low emitter efficiency," in *Proc. ISPSD'93*, Monterey, CA, 1993, pp. 30–34.

[4] A. R. Hefner, "Modeling buffer layer IGBT's for circuit simulation," *IEEE Trans. Power Electron.*, vol. 10, pp. 111–123, June 1994.

[5] ——, "A dynamic electro-thermal model for the IGBT," *IEEE Trans. Ind. Applicat.*, vol. 30, pp. 394–405, Mar./Apr. 1994.

[6] R. Kraus, K. Hoffmann, and P. Türkes, "Analysis and modeling of the technology-dependent electrothermal IGBT characteristics," in *Proc. IPEC'95*, Yokohama, Japan, 1995, pp. 1128–1133.

[7] *MicroSim PSpice A/D Reference Manual*, MicroSim Corp., Irvine, CA, Apr. 1996, p. 210.

[8] *Saber 4.0 User's Manual*, Analogy, Inc., now Avant! Inc., Beaverton, OR, 1996.

[9] M. Gallaher and S. Martin, Eds., "Benefit analysis of IGBT power device simulation modeling," Research Triangle Institute Center for Economics Research, Research Triangle Park, NC, NIST Planning Rep. 99-3, Apr. 1999.

[10] NIST/IEEE working group on model validation (1993, Sept.). [Online]. Available: http://ray.eeel.nist.gov/modval.html

[11] K. Wang, F. C. Lee, G. Hua, and D. Borojevic, "A comparative study of switching losses of IGBT's under hard-switching, zero-voltage-switching and zero-current-switching," in *Conf. Rec. IEEE PESC'94*, June 1994, pp. 1196–1204.

[12] A. N. Githiari, B. Gordon, R. McMahon, Z.-M. Li, and P. Mawby, "A comparison of IGBT models for use in circuit design," *IEEE Trans. Power Electron.*, vol. 14, pp. 607–613, July 1999.

[13] A. Elasser, V. Parthasarathy, and D. A. Torrey, "A study of the internal device dynamics of punch-through IGBT's under zero-current switching," *IEEE Trans. Power Electron.*, vol. 12, pp. 21–35, Jan. 1997.

[14] D. W. Berning and A. R. Hefner, "IGBT model validation," *IEEE Ind. Applicat. Mag.*, vol. 4, pp. 23–34, Nov./Dec. 1998.

[15] A. R. Hefner, "Semiconductor measurement technology," in *INSTANT—IGBT Network Simulation and Transient ANalysis Tool*. Gaithersburg, MD: National Inst. of Standards and Technology, June 1992, pp. 400–488.

[16] A. R. Hefner and D. M. Diebolt, "An experimentally verified IGBT model implemented in the saber circuit simulator," in *Conf. Rec. IEEE PESC'91*, June 1991, pp. 10–19.

[17] A. R. Hefner, "A dynamic electro-thermalmodel for the IGBT," in *Conf. Rec. IEEE-IAS Annu. Meeting*, Oct. 1992, pp. 1094–1104.

[18] D. W. Berning and A. R. Hefner, "IGBT half-bridge shoot-through characterization for model validation," in *Conf. Rec. IEEE-IAS Annu. Meeting*, Oct. 1996, pp. 1491–1499.

David W. Berning was born in Cincinnati, OH, in 1951. He received the B.S. degree in physics from the University of Maryland, College Park, in 1973.

In 1974, he joined the National Bureau of Standards (now the National Institute of Standards and Technology), Gaithersburg, MD. Much of his career has focused on semiconductor device reliability, first using laser-scanning techniques to probe active devices, and later using electrical methods to explore safe operating area for power devices. He is currently involved in developing techniques for characterizing high-voltage high-speed SiC power diodes and MOSFETs. He is the holder of three U.S. patents in the area of audio amplifier design.

Allen R. Hefner, Jr. (S'84–M'84–SM'93) was born in Washington, DC, in 1959. He received the B.S., M.S., and Ph.D. degrees in electrical engineering from the University of Maryland, College Park, in 1983, 1985, and 1987, respectively.

In 1983, he joined the Semiconductor Electronics Division, National Institute of Standards and Technology (NIST), Gaithersburg, MD, where he is presently the Group Leader for the NIST Semiconductor Electronics Division's Device Technology Group and the Project Leader for the Metrology for Simulation and Computer Aided Design Project. He has also served as a member of the NIST Research Advisory Committee (1997–1999). His research interests include characterization, modeling, and circuit utilization of power semiconductor devices.

Dr. Hefner received a U.S. Department of Commerce Silver Medal Award in 1993 for his pioneering work in modeling advanced power semiconductor devices for electrothermal circuit simulation. He is also the recipient of the 1996 NIST Applied Research Award for development and transfer of the IGBT model to circuit simulator software vendors. He is the author of 50 publications in IEEE TRANSACTIONS and conference proceedings and is the recipient of an IEEE Industry Applications Society (IAS) Prize Paper Award. He has presented 25 invited seminars and was an instructor for the IEEE Power Electronic Specialists Conference tutorial course (1991 and 1993) and for the IAS Annual Meeting tutorial course (1994). He has served as a Program Committee Member for the IEEE Power Electronics Specialists Conference (1991–1999) and as the Transactions Review Chairman for the Power Electronics Devices and Components Committee of the IAS (1989–1997). He has also served as the IEEE Electron Device Society Standards Technical Committee Chairman (1996–2000) and is a member of the Power Devices and Integrated Circuits Technical Committee of the IEEE Electron Devices Society.